

# Effects of Gravitational Microlensing on P-Cygni Profiles of Type Ia Supernovae

Hamed Bagherpour <sup>1</sup>, David Branch <sup>2</sup>, Ronald Kantowski <sup>3</sup>

*University of Oklahoma, Department of Physics and Astronomy,  
Norman, OK 73019, USA*

## ABSTRACT

A brief description of the deformed spectra of microlensed SNe Ia is presented. We show that microlensing amplification can have significant effects on line profiles. The resonance-scattering code SYNOW is used to compute the intensity profile in the rest frame of the supernova. The observed (microlensed) spectral lines are predicted assuming a simple stellar-size deflector, and are compared to unlensed cases to show the effects microlensing by solar-size deflectors can have on spectral lines. We limit our work to spherically symmetric deflectors.

*Subject headings:* gravitational lensing — supernovae: general

## 1. Introduction

It is known that amplification of a light source due to microlensing can affect the spectral line profiles if different parts of the profile originate from different emitting regions of the source (e.g., if the emitting region has a ring-like structure) and if the sizes of these regions are comparable to the characteristic lensing radius (Kayser, Refsdal, & Stabell 1986). Evidence of such effects on line profiles of broad-absorption-line (BAL) quasars was suggested by spectroscopic observations of the multiple images of the strongly lensed quasar H1413+117 (Angonin et al. 1990). Spectral differences observed between the four images of this quasar were investigated by Hutsemékers (1993) using the lens model of Chang & Refsdal (1984).

One expects these ‘chromatic amplifications’ to be observed in a microlensed type Ia supernova as well. SNe Ia are well-studied extended light sources consisting of a central

---

<sup>1</sup>hamed@nhn.ou.edu

<sup>2</sup>branch@nhn.ou.edu

<sup>3</sup>kantowski@nhn.ou.edu

continuum source surrounded by a rapidly expanding atmosphere. The atmosphere accounts for the formation of the observed P-Cygni profiles in the spectral lines of these objects. In § 2 we show how microlensing by a simple (point-mass) Schwarzschild deflector can deform these P-Cygni line profiles. Results of lensing a source at  $z_s = 1$  by a deflector at  $z_d = 0.05$  are presented in § 3. A flat Friedmann-Lamaitre-Robertson-Walker cosmological model with  $\Omega_m = 0.3$ ,  $\Omega_\Lambda = 0.7$ , and  $h_{100} = 0.67$  is assumed to calculate source and deflector distances.

## 2. Microlensing of a Supernova as an Extended Source

### 2.1. Line Profiles of Type Ia Supernovae

P-Cygni profiles are characterized by emission lines together with corresponding blueshifted absorption lines. The latter is produced by material moving away from the source with either relativistic velocities (Hutsemékers & Surdej 1990) or nonrelativistic velocities (Beals 1929). For an explosive expansion the material in each plane perpendicular to the line of sight has a fixed component of velocity  $V_r$  toward the observer (Fig. 1).

Using the normalized, projected radius  $P$  (i.e., the photosphere at  $P = 1$ , see Fig. 1), the unlensed flux is defined as

$$F_\lambda = \int_0^{2\pi} \int_0^{P_{max}} I_\lambda(P, \theta) P dP d\theta, \quad (1)$$

where  $P_{max}$  is the normalized, projected radius of the supernova and the plane polar angle  $\theta$  is measured in the projected source plane.

To compute the intensity  $I_\lambda$ , we used a resonance-scattering synthetic spectrum produced with the fast, parameterized supernova synthetic-spectrum SYNOW. This code is often used for making and studying line identifications and initial coarse analysis of the spectra during the photospheric phase of the supernova (Branch et al. 2003, 2005). The code assumes a spherically symmetric and sharp photosphere that emits a blackbody continuum characterized by temperature  $T_{bb}$ .

In SYNOW, the expansion velocity is proportional to radius (homologous expansion:  $v = r/t$ ), as expected for matter coasting at a fixed velocity after an impulsive ejection with a range of velocities. Line formation is treated in the Sobolev approximation (Sobolev 1958) and occurs by resonance scattering of photons originating from the photosphere. Line blending is treated in a precise way, within the context of the Sobolev approximation. Each line optical depth  $\tau$  is taken to decrease exponentially with radius [See Jeffery & Branch (1990) and Fisher (2000) for more details]. The code does not calculate ionization ratios or

rate equations; it takes line identifications to estimate the velocity at the photosphere and the velocity interval within which ions are detected. These quantities give constraints on the composition structure of the ejected matter.

SYNOW calculates the intensity emitted from each zone (concentric annuli) of the projected source. These intensity profiles show the absorption features for various  $P < 1$  as well as emission features for  $P > 1$ . The weighted sum of these intensities over the projected surface of the supernova (eq. [1]) gives the synthetic flux profile. Figure 2 shows the calculated intensity profiles of sodium. These profiles are obtained for optical depths of  $\tau = 1$  (upper panel) and  $\tau = 1,000$  (lower panel). The intensities are calculated for  $P > 1$ ,  $P = 0$ , and  $P$  just below 1. The asymmetry seen in the emission features is caused by applying the relativistic Sobolev method (Jeffery 1993) in the SYNOW code which, in turn, introduces a Doppler boosting in the profiles. Note that to relate the quantities in the comoving and observer frame, one has to use the transformation

$$I_\lambda = I_{\lambda_o} \frac{\lambda_o^5}{\lambda^5}, \quad (2)$$

where the quantities with subscript ‘o’ denote those measured in the comoving frame (Mihalas 1978).

## 2.2. Differential Amplification

Micro lensing of an extended source such as a type Ia supernova by an isolated compact mass results in two images, both in line with the source and deflector projected on the sky plane. The ‘primary’ image,  $r_p$ , lies on the same side of the deflector as the source while the ‘secondary’ image,  $r_s$ , is on the opposite side. For solar-mass size deflector the angular separation of the two images is of the order of micro arcseconds and as a result, they are seen as a single object as expected for microlensing events (Schneider, Ehlers, & Falco 1992). The apparent brightness of this ‘single’ image differs from that of the unlensed source and is proportional to the apparent area of the image, meaning that the brightness of a source is amplified by a factor

$$Amp = \frac{A_o}{A}, \quad (3)$$

where  $A_o$  is the area of the image and  $A$  is the area of the source both projected on the sky plane. See Bagherpour et al. (2005) for details.

If the different parts of the spectral profile come from different parts of the source (which is the case for the concentric annuli of an isotropically expanding type Ia supernova), and if the emitting regions are not much bigger than the characteristic lensing radius (Kayser,

Refsdal, & Stabell 1986), one may expect to see not only a rescaling in the observed flux, but also a deformation in the line profiles. For a lensed supernova, the observed line profile becomes

$$F_\lambda = \int_0^{2\pi} \int_0^{P_{max}} I_\lambda(P, \theta) Amp(P, \theta) P dP d\theta, \quad (4)$$

where  $Amp(P, \theta)$  is the amplification of the surface element centered at point  $(P, \theta)$ . Assuming that a supernova explodes isotropically, the altered flux becomes

$$F_\lambda = \int_0^{P_{max}} I_\lambda(P) Amp(P) P dP, \quad (5)$$

where

$$Amp(P) \equiv \int_0^{2\pi} Amp(P, \theta) d\theta. \quad (6)$$

For an annulus with the width  $\delta P$  bounded by inner and outer radii of  $P_- \equiv P - \frac{\delta P}{2}$  and  $P_+ \equiv P + \frac{\delta P}{2}$ , the amplification becomes

$$Amp(P) = \frac{S_+ - S_-}{\pi (P_+^2 - P_-^2)}, \quad (7)$$

where

$$S_\pm = \int_{-\frac{\pi}{2}}^{\frac{\pi}{2}} P_\pm (P_\pm + l \sin \varphi) \sqrt{1 + \frac{4r_E^2}{l^2 + P_\pm^2 + 2P_\pm l \sin \varphi}} d\varphi. \quad (8)$$

(See Bagherpour et al. (2005)). In the above equation,  $l$  is the distance between the deflector and supernova, and  $r_E$  is the radius of Einstein ring. All distances are projected on the deflector plane.

The amplification can be calculated using elliptical integrals (Witt & Mao 1994; Mao & Witt 1998). Figure 3 shows amplification as a function of the expansion velocity of the projected annuli for several values of  $l$  in terms of the Einstein ring  $r_E$ . Notice that each curve peaks at the velocity corresponding to the annulus which is partially obscured by the deflector.

### 3. Lensed Profiles

In this section we calculate the deformed spectral profiles of microlensed SNe Ia. To calculate the differential amplification, we need to specify the distance  $l$  between the supernova and the deflector projected on the plane of the deflector (sky plane), normalized by the Einstein ring radius  $r_E$ ,

$$u_A \equiv \frac{l}{r_E}. \quad (9)$$

The radius  $r_E$  is determined by the mass of the deflector  $m_d$  and the weighted distance (of luminosity distances)  $D$ ,

$$r_E = \sqrt{\frac{4Gm_d D}{c^2}}, \quad (10)$$

where  $D \equiv D_{ds}D_d/D_s$  in which,  $D_s$ ,  $D_d$ , and  $D_{ds}$  are the respective observer-source, observer-deflector, and deflector-source distances. These are angular size distances calculated adopting a  $(\Omega_m, \Omega_\Lambda, h) = (0.3, 0.7, 0.67)$  cosmology. We assume that the source is at redshift  $z_s = 1.0$  and is lensed by a deflector located at redshift  $z_d = 0.05$ . The point-like deflector has a mass of  $1 M_\odot$  and when positioned at different projected distances it magnifies parts of the extended source differently. The Einstein radius  $r_E$  for the above deflector mass and distances is  $\sim 1301$  AU.

We have considered an SN Ia with fixed radius of 178 AU, corresponding to that of a supernova with a maximum atmospheric speed of  $30,000 \text{ km s}^{-1}$  at eighteen days after the explosion. The radius of the supernova projected on the deflector plane,  $r_{SN}$ , is  $\sim 20$  AU, with a photospheric radius of  $r_{Ph} \approx 8$  AU. The black body continuum temperature  $T_{bb}$  is taken to be 14,000 degrees. Optical depths  $\tau$  are taken to vary exponentially for each line as

$$\tau(v) = \tau_o \exp\left(-\frac{v}{v_e}\right), \quad (11)$$

where  $v$  is the expansion velocity of each layer and  $v_e$  is the corresponding e-folding velocity (e.g.,  $1,000 \text{ km s}^{-1}$  for sodium).

We used SYNOW to calculate the unlensed sodium lines as well as their corresponding lensed profile for different optical depths  $\tau_o$  and normalized distances  $u_A$  to show the effect microlensing can have on a single, clean line. Figures 4 through 7 show the results of such calculations for  $\tau_o = 1$  and 1,000, and  $u_A = 0$  and  $1/128$  ( $\approx 0.008$ )<sup>1</sup>. In these diagrams, flux is plotted in an arbitrary unit as a function of wavelength. As can be seen in Figure 4, the emission feature is reduced with respect to the absorption feature because the  $P < 1$  region is magnified much more than the  $P > 1$  region. The narrowing of the absorption dip as well as an overall shift of the lensed curve to the left is due to the extreme amplification of the  $P = 1$  annulus. This is the result of the source-deflector alignment (Fig. 3) which causes the area with the highest blueshift ( $P = 1$ ) to get the highest amplification. With  $u_A = 1/128$  (Fig. 5), the emission feature of the apparent line profile is magnified while the absorption feature does not change remarkably because the amplification curve maximizes outside  $P < 1$  region and flattens inside (Fig. 3). Figure 6 is the same as Figure 4 with  $\tau = 1,000$ . In this figure, we once again notice the effect of extreme amplification of the

---

<sup>1</sup>We changed  $u_A$  in terms of negative powers of 2 to let it go to zero asymptotically.

central zone of the source in the form of a slight shift of the apparent curve toward lower wavelengths. Contrary to Figure 4, we do not encounter sharp dips here because each dip in the (unlensed) intensity curve is  $7,000 \text{ km s}^{-1}$  wide. As expected, moving the deflector away from the line of sight to the source results in a stronger emission component while the absorption dip does not vary remarkably (Fig. 7).

Figures 8 and 9 show the same calculations as those of Figures 4 to 7 for a SYNOW synthetic spectrum that resembles that of a SN Ia near maximum light with  $u_A = 0$  and  $1/128$ , respectively. We have normalized the lensed profile at  $\lambda = 7,000 \text{ \AA}$ . Because noticeable deformation of the profiles appear only when the deflector is almost aligned with the source (small values of  $u_A$ ), we did not include results for  $u_A > 1/128$  (i.e.,  $l > 10.17 \text{ AU}$ ). With  $u_A = 0$  (Fig. 8), central parts of supernova are amplified more than the rest which, as explained for Figures 4 and 6, results in a slight shift toward lower wavelengths. Again, emission features are demagnified with respect to the absorption components. The observed spectral lines show sharp dips because the input value of optical depth  $\tau$  for each line is not too high. Figure 9 is the same as Figure 8 but with  $u_A = 1/128$ . Here, the light coming from the  $P > 1$  area carrying emission features has higher amplification compared to the blueshifted light emitted from  $P < 1$  and, as expected, the emission component of the P-Cygni features is magnified more than the absorption part.

The change in the profiles can, in general, be summarized as a net increase or decrease of the absorption component relative to the emission one. The apparent change in either component may be so strong that an emission feature could look like a typical P-Cygni profile. To see this effect, the projected source (supernova) must be very close to the deflector on the sky plane ( $l \ll r_E$ ). Larger impact parameters produce less dramatic deviations from the unlensed profile and could easily be attributed to the intrinsic diversity in spectra of type Ia supernovae rather than gravitational lensing. The deflector redshift used here ( $z_d = 0.05$ ) is not the most likely redshift for microlensing but results in a remarkable amplification gradient necessary for noticeable deformation of P-Cygni profiles. In general, the probability of microlensing cosmologically distant light source is not negligible, and can exceed 1% for a source located at  $z_s = 1$  and beyond (Myers et al. 1995; Wyithe & Turner 2002; Zakharov, Popović, & Jovanović 2004). However, for the small values of  $u_A$  used here the probability of observing such deformations drops below 0.001% (Bagherpour et al. 2005).

It should be noted that we have ignored any contribution to lensing from nearby stars and the deflector’s parent galaxy. For most microlensing events the amplification due to the host galaxy is expected to introduce a small amplification gradient across the supernova which merely rescales the line profile without introducing any significant deformation effects. Macrolensing by the galaxy should mainly bias the supernovae detection. The rescaling effect

is compensated for by normalizing the lensed profile in order to compare the apparent and unlensed profiles, as done in Figures 4 through 9. When large amplification gradients are introduced, either by the galaxy or by microlensing stars nearby, a more complicated lens models will be required.

#### 4. Conclusion

We have shown that microlensing can significantly affect the P-Cygni profile of a cosmologically distant type Ia supernova. We restricted our calculation to  $z_s = 1$  and  $z_d = 0.05$  in the commonly used  $\Omega_m = 0.3$ ,  $\Omega_\Lambda = 0.7$  flat cosmological model with  $h_{100} = 0.67$ . We found that microlensing can not only increase the flux magnitude but also can cause a change in its line profiles. Microlensing can cause the features in the spectral lines to be blueshifted with respect to the original spectrum and in general, results in a net increase or decrease of the absorption component relative to the emission component.

We calculated the deformed line profiles for special cases where the deflector is extremely close to the line of sight to the source. Due to the low probability of microlensing events occurring with such small values of  $u_A$ , a large population of supernovae (around  $10^5$ ) would have to be surveyed to observe a single case of deformation in P-Cygni profiles of type Ia SNe. Also, large deformations demand using more complicated lensing models.

H. B. wishes to thank Darrin Casebeer for helpful discussions. This work was in part supported by NSF grant AST0204771 and NASA grant NNG04GD36G.

#### REFERENCES

- Angonin, M., et al. 1990, A&A, 233, L5  
Bagherpour, H., et al. 2005, ApJ, submitted  
Beals, C. 1929, MNRAS, 90, 202  
Branch, D., et al. 2003, AJ, 126, 1489  
Branch, D., et al. 2005, PASP, 117, 545  
Chang, K., & Refsdal, S. 1984, A&A, 132, 168  
Fisher, A. 2000, PhD thesis, University of Oklahoma

- Hutsemékers, D., & Surdej, J. 1990, *ApJ*, 361, 367
- Hutsemékers, D., Surdej, J., & Van Drom, E. 1992 *Lecture Notes in Physics, Gravitational Lenses*, ed. R. Kayser et al. (Berlin: Springer-Verlag)
- Hutsemékers, D. 1993, *A&A*, 280, 435
- Jeffery, D., & Branch, D. 1990, *Jerusalem Winter School for Theoretical Physics, Vol. 6*, ed. J. C. Wheeler, S. Weinberg (Singapore: World Scientific)
- Jeffery, D. 1993, *ApJ*, 415, 734
- Kayser, R., Refsdal, S., & Stabell, R. 1986, *A&A*, 166, 36
- Mao, S., & Witt, H. J. 1998, *MNRAS*, 300, 1041
- Mihalas, D. 1978, *Stellar Atmospheres* (San Francisco: Freeman)
- Myers, S. T., et al. 1995, *ApJ*, 447, 15
- Schneider, P., Ehlers, J., & Falco, E. E. 1992, *Gravitational Lenses* (Berlin: Springer-Verlag)
- Sobolev, V. V. 1958, *Theoretical Astrophysics*, ed. V A. Ambartsumyan (London: Pergamon)
- Witt, H. J., & Mao, S. 1994, *ApJ*, 430, 505
- Wyithe, J. S. B., Turner, E. L. 2002, *ApJ*, 567, 18
- Zakharov, A. F., Popović, L. Č., & Jovanović, P. 2004, *A&A*, 420, 881

Fig. 1.—

Schematic view of a type Ia supernova as seen by an observer. The normalized radius  $P$  and planar speed  $V_r$  are shown.

Fig. 2.—

Synthetic intensity profile of a type Ia supernova, showing absorption and emission features for  $P < 1$ ,  $P > 1$ , and  $P$  just below 1 for  $\tau = 1$  (upper panel) and  $\tau = 1,000$  (lower panel). The emission feature in the upper panel is scaled up.

Fig. 3.—

This figure shows the amplification curves of any point on the projected source as a function of expansion velocity for different values of  $l$ . The value of photospheric expansion speed determines the zone (absorption or emission) with higher amplification.

Fig. 4.—

Amplified line profile of sodium for  $\tau = 1$  and  $u_A = 0$ . The deflector has a mass of  $1M_\odot$ .

Fig. 5.—

Same as Fig. 4, with  $\tau = 1$  and  $u_A = 1/128$ .

Fig. 6.—

Same as Fig. 4, with  $\tau = 1,000$  and  $u_A = 0$ .

Fig. 7.—

Same as Fig. 4, with  $\tau = 1,000$  and  $u_A = 1/128$ .

Fig. 8.—

Amplified spectral lines of a SYNOW spectrum that resembles the maximum-light spectrum of a SN Ia, with  $u_A = 0$  and  $m_d = 1M_\odot$

Fig. 9.—

Same as Fig. 8, with  $u_A = 1/128$ .

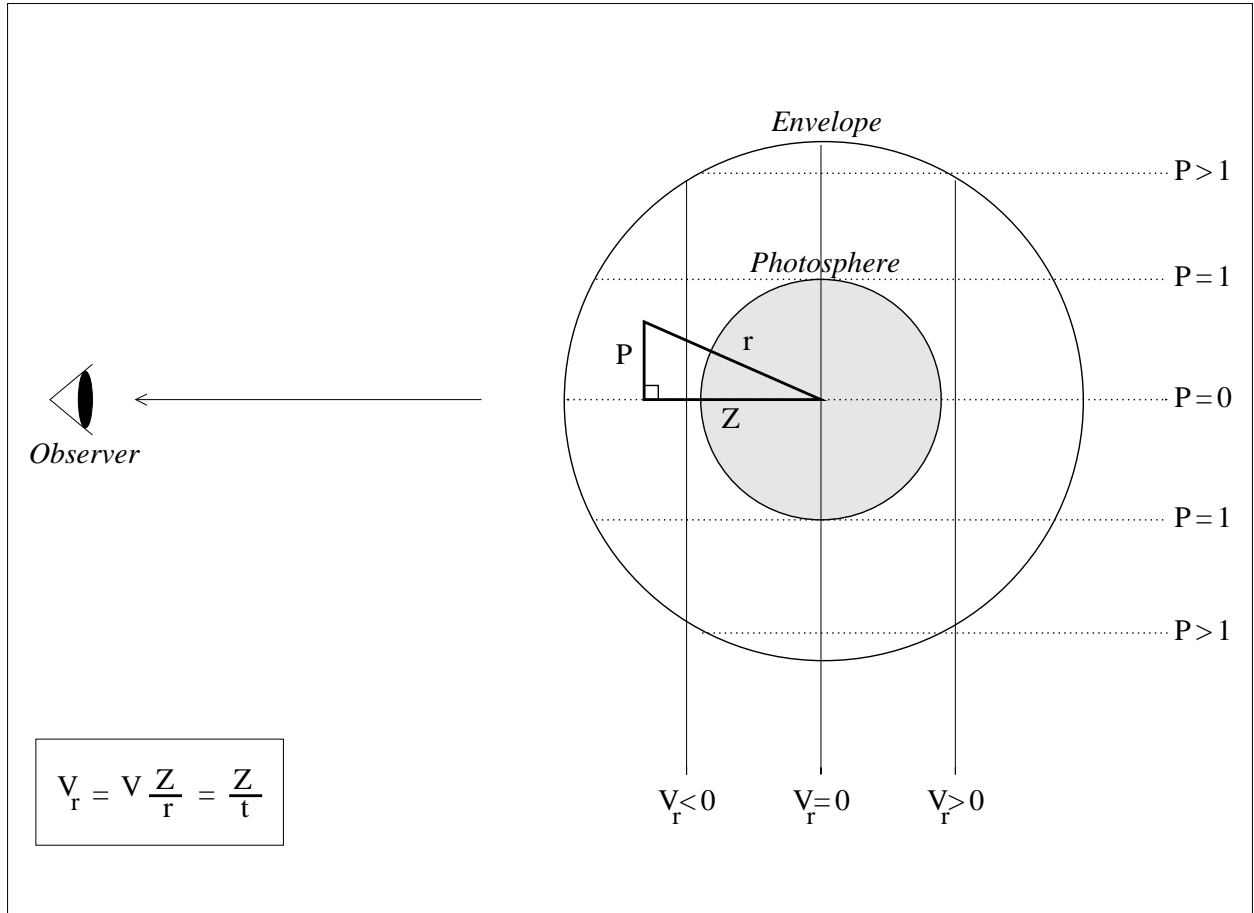


Figure 1

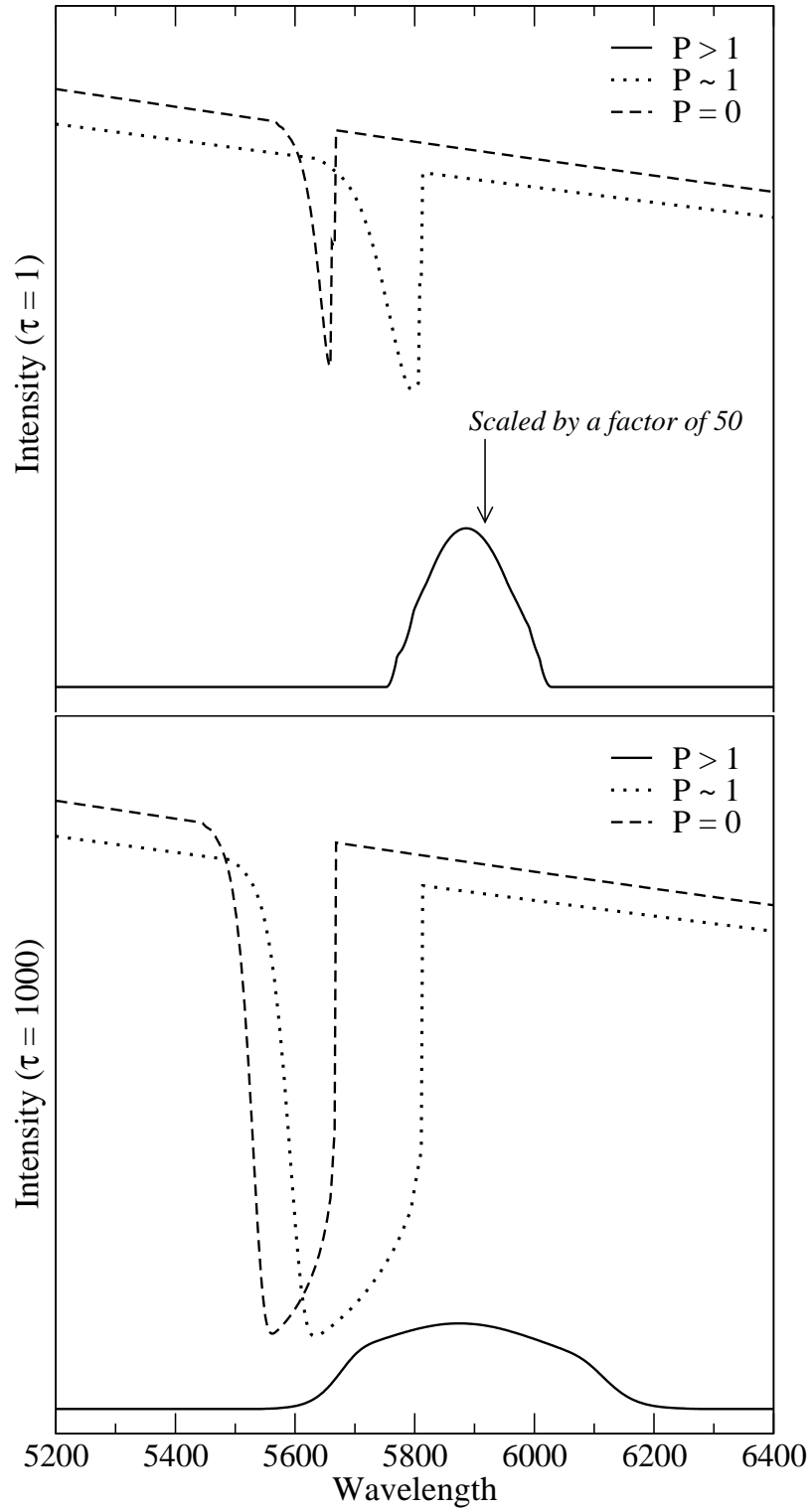


Figure 2

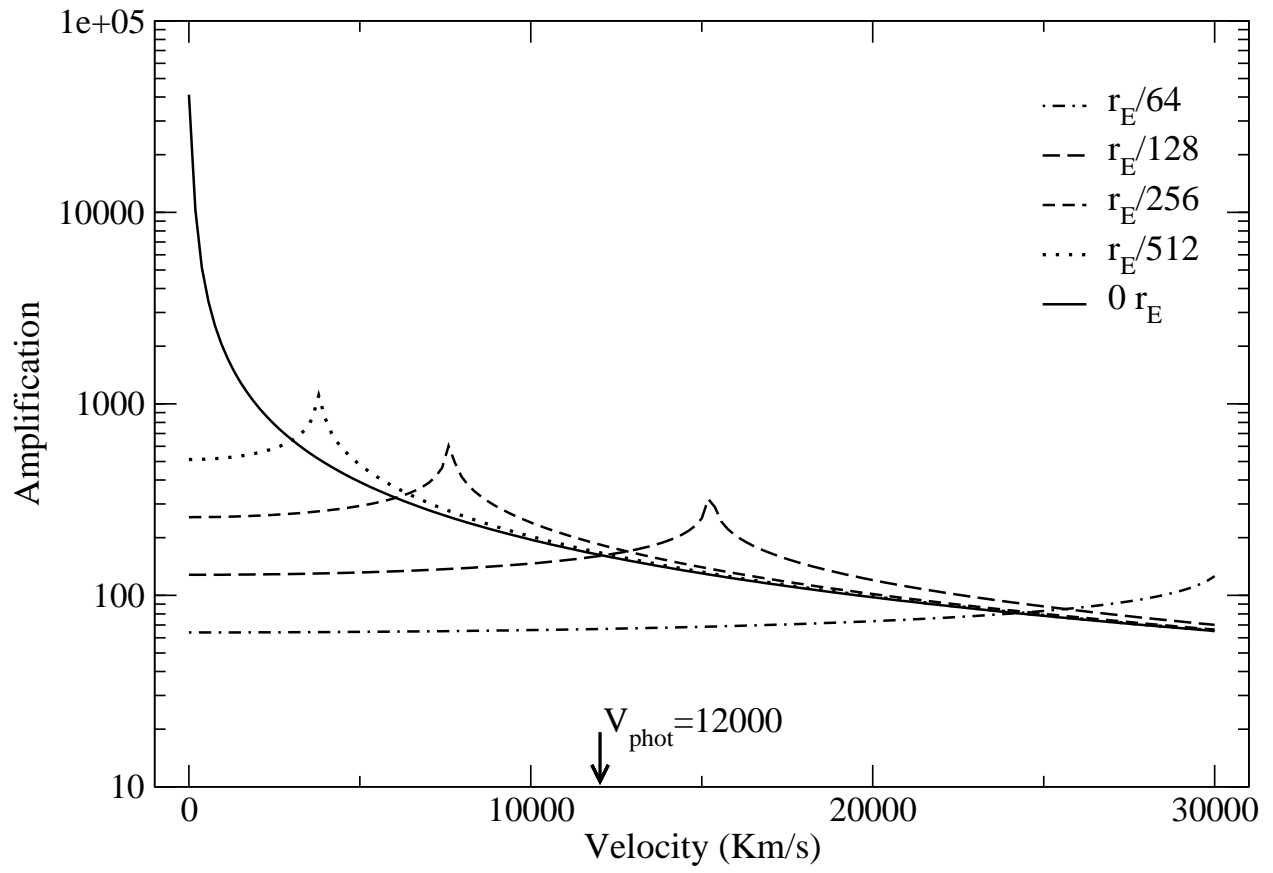


Figure 3

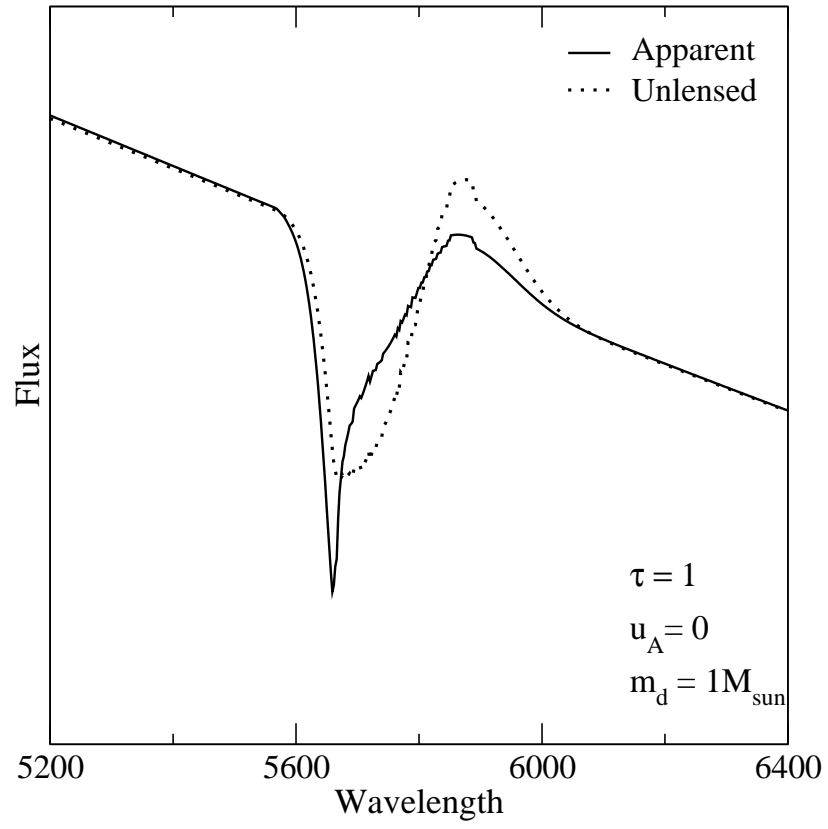


Figure 4

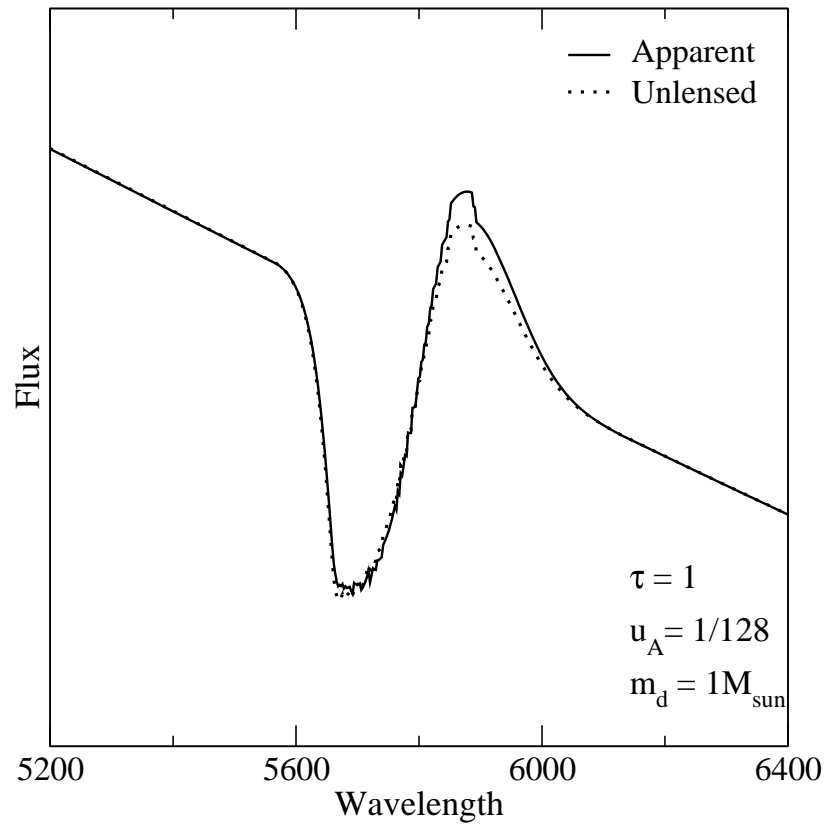


Figure 5

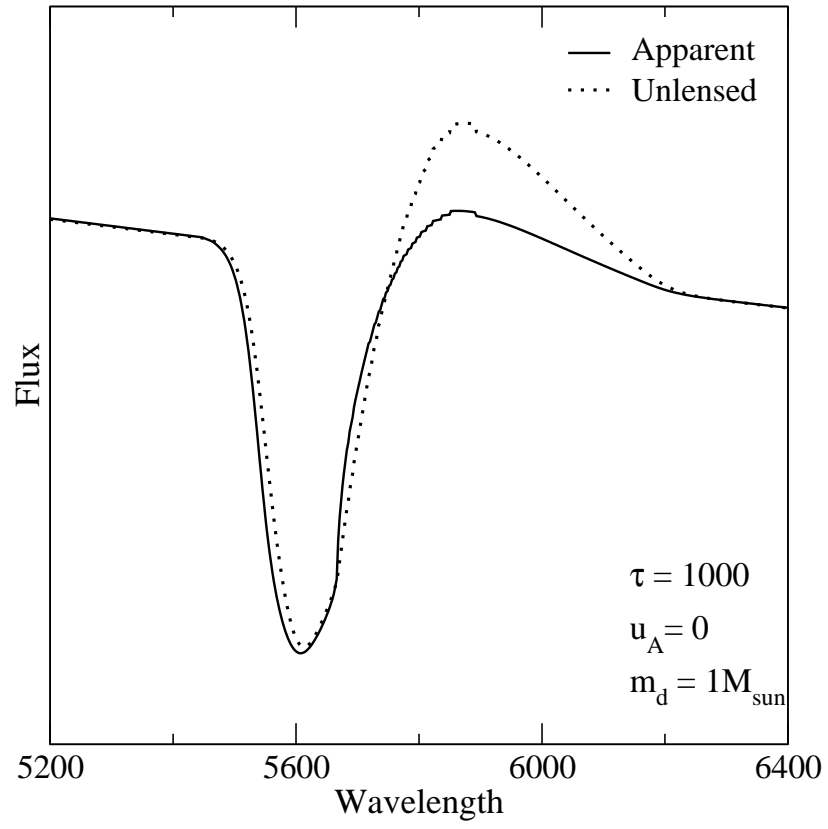


Figure 6

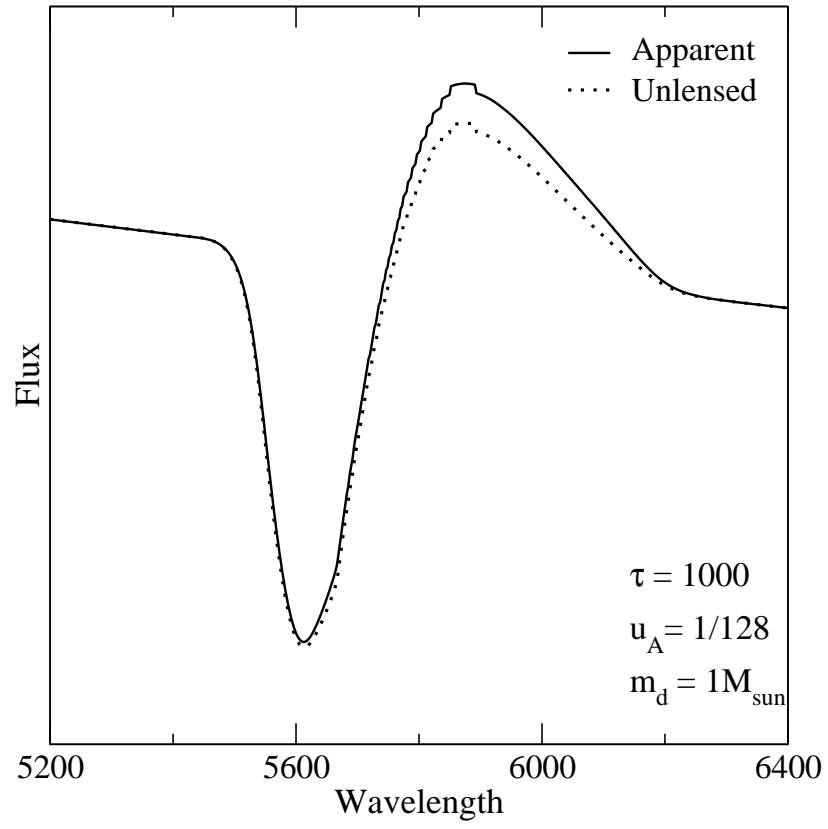


Figure 7

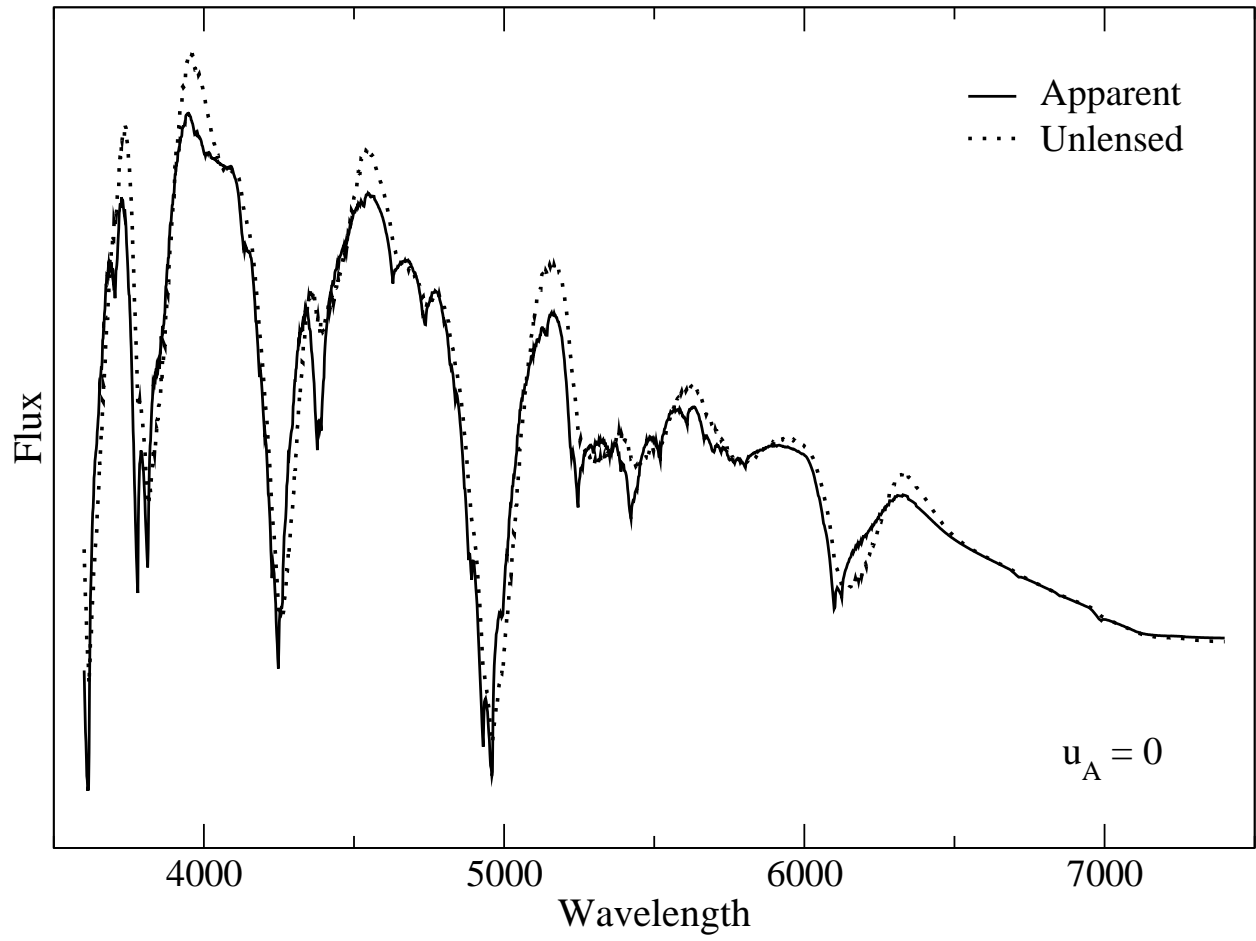


Figure 8

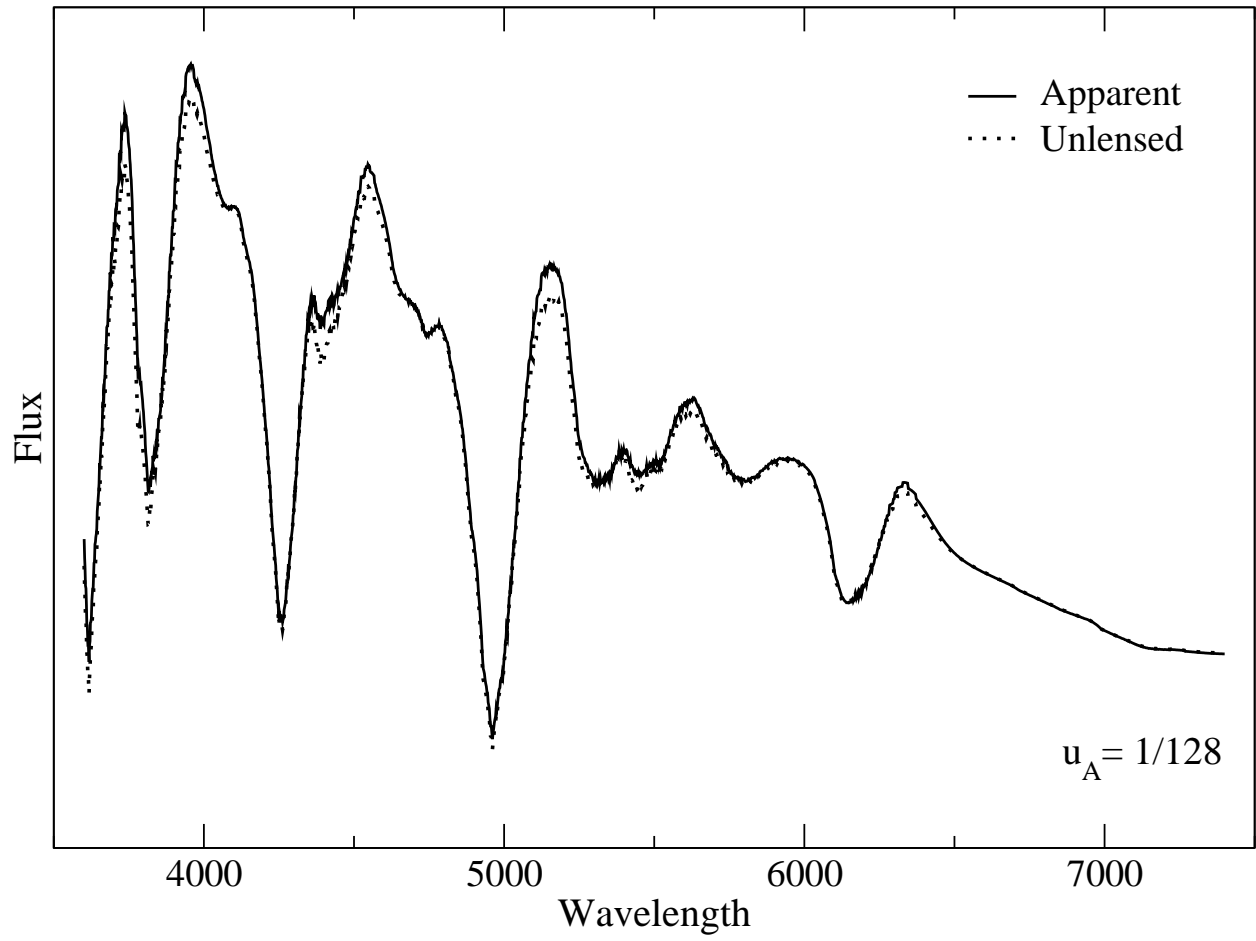


Figure 9